Model-independent determination of the dipole response of ^{66}Zn using quasimonoenergetic and linearly polarized photon beams

D. Savran,[1,*] J. Isaak,[2] R. Schwengner,[3] R. Massarczyk,[4] M. Scheck,[5,6] W. Tornow,[7,8] G. Battaglia,[9] T. Beck,[10] S. W. Finch,[7,8] C. Fransen,[11] U. Friman-Gayer,[7,8] R. Gonzalez,[8,12] E. Hoemann,[11] R. V. F. Janssens,[8,12] S. R. Johnson,[8,12] M. D. Jones,[8,12] J. Kleemann,[2] Krishichayan,[7,8] D. R. Little,[8,12] D. O'Donnell,[5,6] O. Papst,[2] N. Pietralla,[2] J. Sinclair,[5,6] V. Werner,[2] O. Wieland,[13] and J. Wilhelmy[11]

[1]*GSI Helmholtzzentrum für Schwerionenforschung GmbH, 64291 Darmstadt, Germany*
[2]*Technische Universität Darmstadt, Department of Physics, Institute for Nuclear Physics, 64289 Darmstadt, Germany*
[3]*Helmholtz-Zentrum Dresden-Rossendorf, 01328 Dresden, Germany*
[4]*Los Alamos National Laboratory, Los Alamos, New Mexico 87545, USA*
[5]*CEPS, University of the West of Scotland, Paisley PA1 2BE, United Kingdom*
[6]*SUPA, Scottish Universities Physics Alliance, United Kingdom*
[7]*Department of Physics, Duke University, Durham, North Carolina 27708, USA*
[8]*Triangle Universities Nuclear Laboratory, Durham, North Carolina 27708, USA*
[9]*University of Strathclyde, Glasgow G4 0NG, United Kingdom*
[10]*Facility for Rare Isotope Beams, Michigan State University, East Lansing, Michigan 48824, USA*
[11]*Institut für Kernphysik, Universität zu Köln, 50937 Köln, Germany*
[12]*Department of Physics and Astronomy, University of North Carolina at Chapel Hill, Chapel Hill, North Carolina 27599, USA*
[13]*Sezione di Milano, INFN, 20133 Milano, Italy*

(Received 20 June 2022; accepted 12 September 2022; published 21 October 2022)

Background: Photon strength functions are an important ingredient in calculations relevant for the nucleosynthesis of heavy elements. The relation to the photoabsorption cross section allows to experimentally constrain photon strength functions by investigating the photoresponse of atomic nuclei.

Purpose: We determine the photoresponse of ^{66}Zn in the energy region of 5.6 MeV to 9.9 MeV and analyze the contribution of the 'elastic' decay channel back to the ground state. In addition, for the elastic channel electric and magnetic dipole transitions were separated.

Methods: Nuclear resonance fluorescence experiments were performed using a linearly polarized quasi-monoenergetic photon beam at the High Intensity γ-ray Source. Photon beam energies from 5.6 to 9.9 MeV with an energy spread of about 3% were selected in steps of 200–300 keV. Two high purity germanium detectors were used for the subsequent γ-ray spectroscopy.

Results: Full photoabsorption cross sections are extracted from the data making use of the monoenergetic character of the photon beam. For the ground-state decay channel, the average contribution of electric and magnetic dipole strengths is disentangled. The average branching ratio back to the ground state is determined as well.

Conclusions: The new results indicate lower cross sections when compared to the values extracted from a former experiment using bremsstrahlung on ^{66}Zn. In the latter, the average branching ratio to the ground state is estimated from statistical-model calculations in order to analyze the data. Corresponding estimates from statistical-model calculations underestimate this branching ratio compared to the values extracted from the present analysis, which would partly explain the high cross sections determined from the bremsstrahlung data.

DOI: 10.1103/PhysRevC.106.044324

I. INTRODUCTION

The modeling of the nucleosynthesis of heavy elements depends on input from nuclear structure and nuclear reaction studies. Statistical model calculations within the Hauser-Feshbach formalism [1] are needed for estimating the relevant reaction rates. One of the important quantities usually used for such calculations is photon strength functions (PSF). These characterize the average probability for the emission and absorption of photons by atomic nuclei. Experimentally, PSF are studied using a variety of reactions, see Refs. [2,3] for an overview. Among the methods, photon-induced reactions offer the possibility to study PSF via their connection to the photoabsorption cross sections σ_γ.

Photonuclear reactions are a common tool to study a variety of nuclear structure phenomena [4]. Due to the well-understood interaction, properties of excited nuclear states can be determined in a model independent way. Below the particle-emission threshold, nuclear resonance fluorescence (NRF) experiments are one of the work horses to provide a broad experimental database.

*d.savran@gsi.de

An interesting region in excitation energy to study the photoresponse of nuclei is from 5 to 10 MeV. In this energy region, the so-called pygmy dipole resonance (PDR) is found in a number of nuclei [5,6]. In the medium mass range, a number of NRF experiments have been performed in order to study the PDR, e.g., in the $Z = 28$ [7–9] isotopes or the $N = 50$ [10–13] isotones. Recent findings on the neutron-number dependence of the low-energy dipole strength near the shell closure $N = 28$ [14–18] indicate its sensitivity to the valence shell and, thus, to single-particle effects [18]. In particular, the Ni and Zn isotopic chains offer the possibility to study the PDR over a broad range of neutron-to-proton ratios in medium mass nuclei.

In order to study the photoresponse of ^{66}Zn in the energy region up to its neutron separation energy ($S_n = 11.06$ MeV), nuclear resonance fluorescence (NRF) experiments were performed at the γELBE facility [19] using broad-band bremsstrahlung as well as at the High Intensity γ-ray Source (HIγS) facility [20] making use of a horizontally linearly polarized, quasi-monoenergetic photon beam produced via laser-Compton backscattering (LCB). In the analysis presented in Ref. [21], the excitation strength of isolated resonances as well as the photoabsorption cross section in bins of 100 keV were extracted from the data taken with bremsstrahlung. The method to determine the latter requires an accurate description of the decay behavior of the photoexcited states within statistical model calculations as described, e.g., in Refs. [12,13,22–26]. The parity-quantum numbers of isolated excited states were determined exploiting the linear polarization of the LCB photon beam produced at HIγS. Furthermore, as shown for other cases [27–32], the monoenergetic character of the LCB photon beam allows to determine the full photoabsorption cross section averaged over the energy profile of the photon beam. At the same time, the average branching ratio needed in the analysis of the bremsstrahlung data can be extracted from the LCB data as well, which allows to verify the accuracy of the calculations within the statistical model. In the present paper, we show the analysis of the LCB data and compare the results with the data presented in [21].

II. EXPERIMENT

An extensive description of the setup and relevant details of the experiments are already given in [21]. Therefore, only a brief summary is provided here. The experiment was performed at the HIγS facility of the Triangle Universities Nuclear Laboratory at Duke University in Durham, NC, USA [20]. At the time of the experiment, two NRF setups were available, the γ^3 setup [33] and a second one located downstream, which was used for the measurement on ^{66}Zn. Two large-volume high purity germanium (HPGe) detectors were positioned at polar angles of 90° with respect to the incoming LCB beam. One HPGe of 100% relative efficiency was placed in the polarization plane (hereafter referred to as *horizontal* detector) and another one of 80% relative efficiency was located perpendicular to the polarization plane (hereafter referred to as *vertical* detector). This geometry is ideal to separate electric dipole ($E1$) from magnetic dipole ($M1$) transitions in an even-even nucleus [34]. The target consisted of 1.4993 g of zinc enriched to 98% in ^{66}Zn, and was formed to a disk with a diameter of 20 mm, which is about the size of the photon beam. For the present analysis, data taken at beam energies of 5.6, 5.75, 5.9, 6.1, 6.3, 6.5, 6.7, 6.9, 7.1, 7.3, 7.5, 7.7, 7.9, 8.15, 8.4, 8.65, 8.9, 9.15, 9.4, 9.65, and 9.9 MeV are considered. For the determination of full energy peak detection efficiencies, a set of calibration measurements have been taken before and after the experiments using standard radioactive sources such as ^{56}Co, ^{60}Co, and ^{152}Eu.

III. ANALYSIS

The present analysis focuses on the extraction of the photoabsorption cross section averaged over the beam energy profiles of the single measurements. For this purpose, we follow mostly the formalism outlined in [32].

The photoabsorption cross section σ_γ can be expressed by the sum of the so-called "elastic" part $\sigma_{\gamma\gamma}$ and the "inelastic" $\sigma_{\gamma\gamma'}$:

$$\begin{aligned}\sigma_\gamma &= \sigma_{\gamma\gamma} + \sigma_{\gamma\gamma'} \\ &= \frac{Y_{0\to x\to 0}}{N_T N_\gamma} + \frac{Y_{0\to x\to i}}{N_T N_\gamma}\end{aligned} \tag{1}$$

with N_T and N_γ being the number of target nuclei and integrated number of impinging photons, respectively. The first part $Y_{0\to x\to 0}$ is the sum over the reaction yields of all photoexcited states x decaying back to the ground state (elastic channel), while $Y_{0\to x\to i}$ represents the sum of all reactions with decays via lower-lying excited states (inelastic channel). The monoenergetic character of the LCB photon beam allows to separately extract both quantities from the measured spectra. The number of target nuclei is calculated from the mass of the NRF target, and the photon intensity can be calibrated via known excitation cross sections of isolated single states determined in the experiment using bremsstrahlung [21].

A. Photon flux

In NRF experiments with bremsstrahlung, absolute excitation cross sections for single excitations can be determined relative to a well-known calibration standard, usually ^{11}B or ^{27}Al. For experiments using quasi-monoenergetic LCB photon beams, this is not possible, since these standards do not have excited states in all the required excitation-energy regions. Moreover, the excitations from the calibration standard might overlap with transitions from the nucleus of interest in the measured γ-ray spectra. However, since energy-integrated cross sections for isolated states of ^{66}Zn have been already determined relative to the calibration standard ^{11}B from NRF measurements with bremsstrahlung [21], these known transitions can be used to calibrate the photon flux in the present case. This is one of the reasons combined experiments using bremsstrahlung and LCB photon beams are so powerful.

In our analysis, we applied the method first presented in [35] and later applied in Ref. [36] as well. Instead of normalizing the measurements for each beam energy separately (as done, e.g., in [32]), in a first step the single measurements were normalized to each other and then normalized to all observed states at all energies with one single parameter.

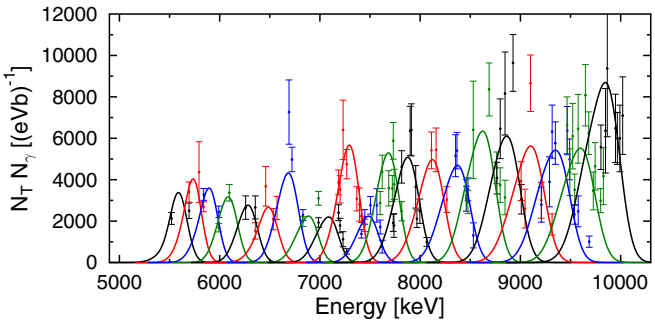

FIG. 1. Normalized LCB beam spectral distributions fit to values extracted from known individual excited states. The different colors are meant to improve visual distinction of the individual data sets and respective beam profiles. See text for details.

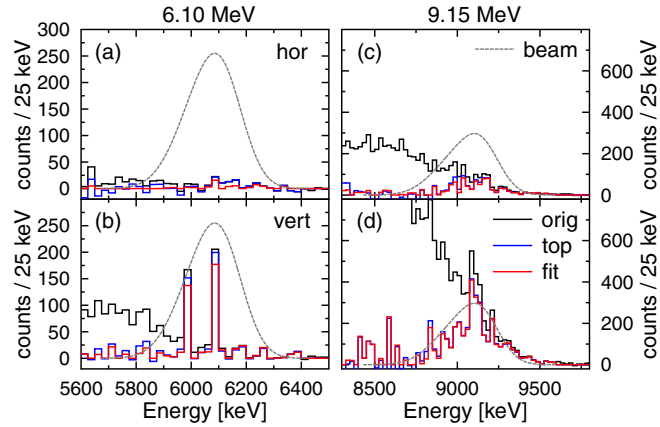

FIG. 2. Spectra recorded with the horizontal (upper panels) and vertical (lower panels) detector, respectively, in 25-keV binning for a LCB beam energy of 6.1 MeV (left) and 9.15 MeV (right). Original spectra are displayed in black, deconvoluted spectra in blue (top-down method) and red (fitting method). In addition, the energy profile of the photon beam is given (dashed line).

The first step can be done by making use of the fact, that the low-energy part of the spectra originates from (atomic) reactions of the photon beam in the target and, thus, is directly proportional to the integrated photon-beam intensity. For the relative normalization, the full geometry was implemented in the *utr* simulation tool kit [37] based on GEANT4 [38–40], and a photon beam with the corresponding energy impinging on the target was simulated. For each beam energy, the simulated spectrum was fitted to the low-energy part of the measured spectrum by the intensity in the 511-keV annihilation peak. It should be noted that this is a very similar approach to that described in Refs. [35,36], with the difference that a well-defined peak is used for normalization instead of a continuous energy region slightly above 511 keV. The extracted factors are proportional to the integrated photon flux in each measurement and were used to normalize the photon flux distributions, which were measured at the beginning of the experiment for each beam-energy setting using an in-beam HPGe detector. After this procedure, the photon-flux distributions, which were normalized relative to each other, differ by only one global scaling factor from the absolute photon-flux intensity. This global factor was determined in the last step by a simultaneous fit of all distributions to the energy-integrated cross section values extracted for known single excitations observed in the spectra. The result is shown in Fig. 1. The values for the integrated photon flux N_γ are calculated by integrating the single photon flux distributions.

The advantage of this procedure is a reduced statistical uncertainty for energy settings, for which only a few known excitations can be used as calibration points shown in Fig. 1. The pure statistical (internal) uncertainty of the global scaling factor in the present case is 1.9%, while the weighted (external) uncertainty is 3.1%, which accounts for the spread of the data about the fit. The latter we used as the uncertainty in the calculation of the cross sections below.

B. Elastic cross section

The state-by-state analysis of isolated resonances does have a sensitivity limit that depends on the background in the γ-ray spectra; i.e., a particular nuclear level needs to have a minimum NRF scattering cross section in order to be observable. Thus, the sum of all observed individual cross sections does not add up to the average elastic cross section $\sigma_{\gamma\gamma}$. In comparison to microscopic models, this can be accounted for by analyzing the fragmentation of the observed dipole strength of individual excitations as done in Ref. [41]. However, a correction of the summed experimental cross section based on this comparison would include a model dependency. The NRF method using an LCB photon beam allows instead a clean determination of the average elastic cross section: Since, in the excitation process, the photon is always fully absorbed, the intensity of the measured γ rays emitted in the subsequent ground-state transitions observed at energies corresponding to the incident LCB beam is directly proportional to the number of elastic NRF reactions $Y_{0\to x\to 0}$:

$$A_{0\to x\to 0} = Y_{0\to x\to 0}\int_{\Delta\Omega} \epsilon(E_x, \Omega) W_{0\to x\to 0} d\Omega \qquad (2)$$

with $A_{0\to x\to 0}$ being the integrated intensity of the spectrum at E_x after correcting for the detector response. The integral in Eq. (2) includes the angular distribution $W_{0\to x\to 0}$ of the NRF reaction and the energy and angle-dependent efficiency $\epsilon(E_x, \Omega)$, which is simulated using GEANT4 as described above. The same simulation is used to determine the energy-dependent detector response, which is used to deconvolute the measured γ-ray spectra, and extract the original intensity. In the present analysis, we used two different deconvolution methods, the top-down method (see, e.g., [24]), and the fitting procedure described in Refs. [42–44]. Figure 2 shows the original spectra for two beam energies for both detectors together with the results of the deconvolution. Parameters within the deconvolution procedures are the used bin size, the low and high energy cut-off and the detector response itself. The parameters were varied as well as the geometry used for the response simulation within reasonable values in order to calculate the systematic uncertainties, which are given in the next section together with the results.

As can be seen in Fig. 2, the intensity in the horizontal detector is much smaller compared to that in the vertical detector (both have about the same efficiency), which indicates that $E1$ is the dominant multipolarity of the elastic photoresponse of ^{66}Zn. However, making use of the angular distribution, the relative contribution of $E1$ and $M1$ can be disentangled by rewriting Eq. (2) as

$$A^i_{0\to x\to 0} = Y_{0\to 1^-\to 0}\int_{\Delta\Omega}\epsilon^i(E_x,\Omega)W^i_{0\to 1^-\to 0}d\Omega + Y_{0\to 1^+\to 0}\int_{\Delta\Omega}\epsilon^i(E_x,\Omega)W^i_{0\to 1^+\to 0}d\Omega, \quad (3)$$

where the index i stands for the two detectors. Thus, measuring the intensities A^i at two different angles is sufficient to separate $E1$ and $M1$ reaction yields; see also Ref. [32]. For the given geometry, $E2$ and $M1$ transitions have the same angular distribution and, thus, cannot be distinguished. However, a considerable contribution of $E2$ at the given excitation energies seems very unlikely and we, thus, neglect this in the following.

C. Inelastic cross section

The determination of the inelastic reaction yield $Y_{0\to x\to i}$ from the primary decay of the initially excited states is difficult, since in most cases the average decay branchings are small [31,42]. However, most of the decay cascades will, at some point, reach the first or one of the other low excited states. Schematically, this is illustrated in Fig. 3: The narrow bandwidth ensures an excitation into a small excitation energy region at E_x, which enables a determination of the full elastic contribution as outlined above. Decay paths going via intermediate excited states will end up in most cases in one of the lowest excited states. Therefore, the intensity of the decay of these excited states is a good approximation of the number of inelastic reactions.

Using this method to measure $\sigma_{\gamma\gamma'}$ has first been proposed by Tonchev *et al.* [27], and was applied in a number of cases, see, e.g., Refs. [8,13,28–30,32].

In the present case of ^{66}Zn, the decay of the first excited 2^+_1 state at 1039 keV is hardly visible above the background at the lowest beam energies, see Fig. 4. With increasing beam energy, the feeding of the 2^+_1 state becomes increasingly pronounced and, thus, the inelastic part of the photoabsorption cross section more important. At energies above 7.5 MeV, two additional peaks appear, that originate from decays of higher-lying states which do not entirely decay via the 2^+_1 state, namely the 2^+_3 at 2780.2 keV and the 1^-_1 state at 3380.9 keV (case 2 in Fig. 3). The intensities of the ground-state decays of these two states are also included in the determination of $\sigma_{\gamma\gamma'}$, but contribute only about 10% even at the highest beam energies. This demonstrates, that cascades completely bypassing the first excited states (case 3 in Fig. 3) will only have a small impact on the measured inelastic cross section. This is the only contribution of $\sigma_{\gamma\gamma'}$ missed in the present analysis.

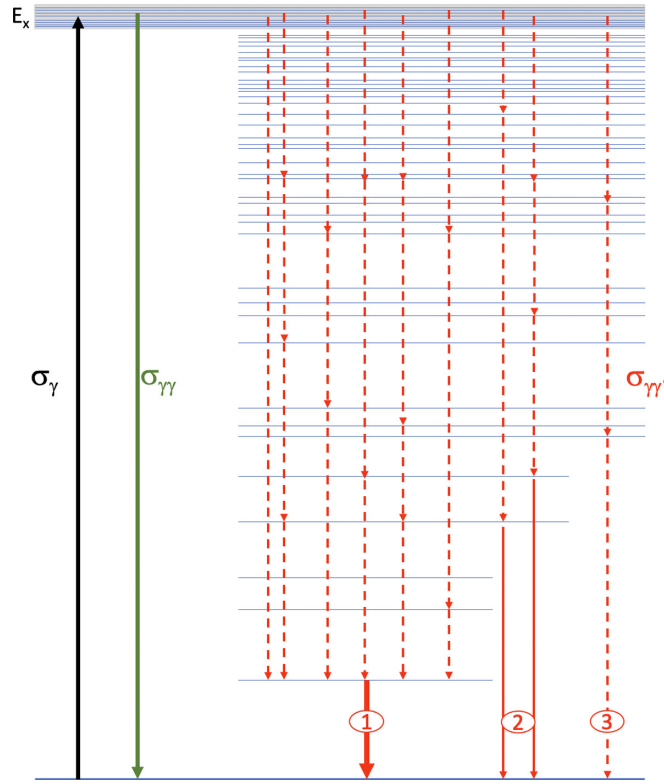

FIG. 3. Illustration of the different decay paths and contributions to the total photoabsorption cross sections σ_γ. After exciting the nucleus to the energy region around E_x defined by the energy profile of the photon beam the primary excited levels can either elastically decay back to the ground state ($\sigma_{\gamma\gamma}$ in green) or inelastically via intermediate states ($\sigma_{\gamma\gamma'}$ in red). Most of the latter intensity is collected by the first excited 2^+ state (case 1). At higher excitation energies ground-state transitions of higher-lying states become visible (case 2), which are added to the $\sigma_{\gamma\gamma'}$ contributions. Possible transition bypassing completely the first excited states stay unobserved (case 3).

IV. RESULTS

In order to determine the integrated intensities $A^i_{0\to x\to 0}$ for the two detectors positioned vertically (i = ver) and

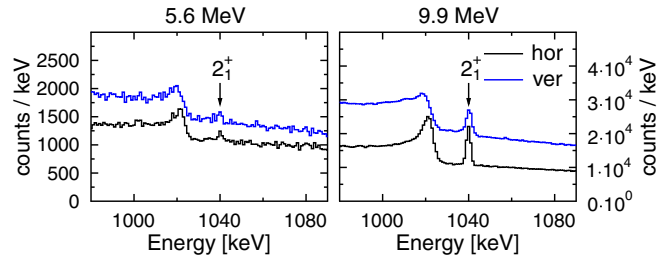

FIG. 4. Measured spectra in the region of the decay energy of the first excited 2^+_1 state at 1039 keV (marked with an arrow). At the lowest beam energy of 5.6 MeV, the peak is hardly visible above the background, while at the highest energy of 9.9 MeV a strong feeding of the state is observed. The structure left to the peak is background resulting from the sum of two 511-keV annihilation γ rays.

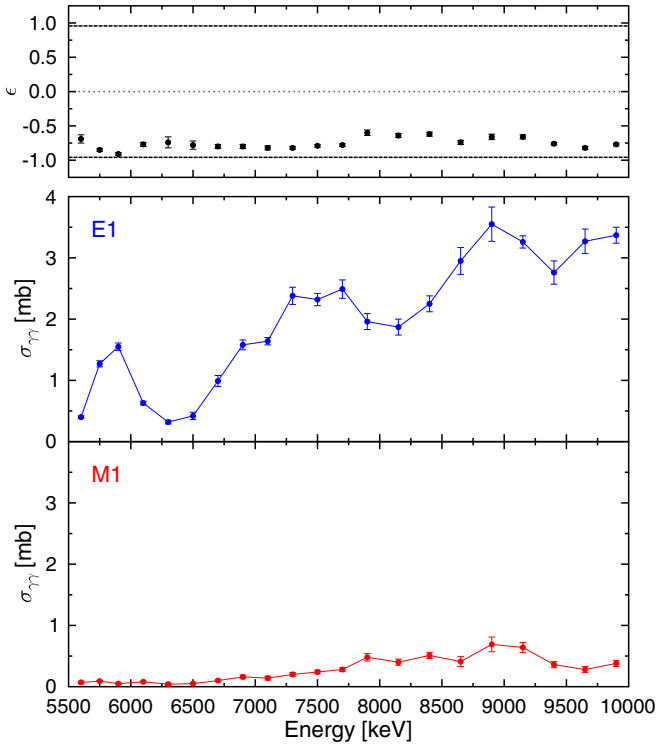

FIG. 5. Upper panel: Average asymmetry determined from Eq. (4). Lower panel: Elastic $E1$ and $M1$ cross section separated by analyzing the angular distribution of the emitted ground-state γ-ray decays. Clearly, $E1$ transitions dominate over the energy region under investigation. The numerical data displayed can be found in Ref. [47].

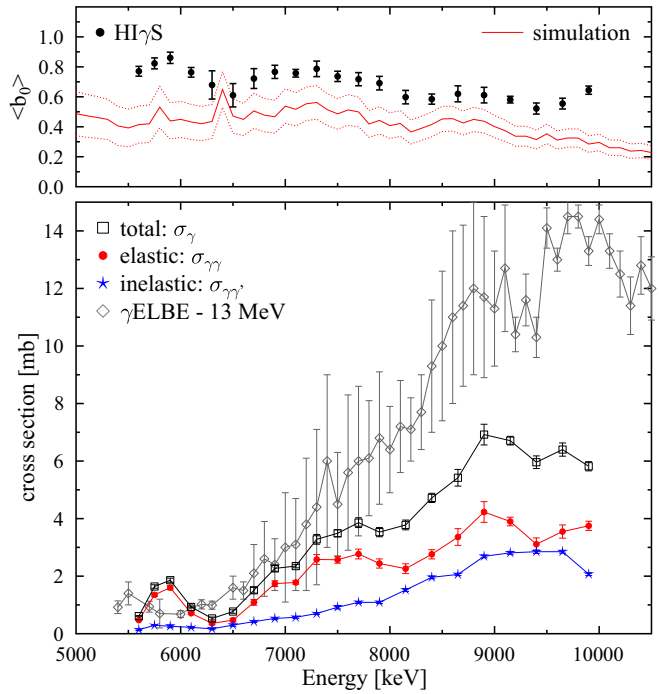

FIG. 6. Lower panel: Elastic, inelastic and total cross sections determined within the present analysis (numerical values can be found in Ref. [47]) compared to the results obtained from bremsstrahlung data taken at γELBE [21]. For our new results systematic uncertainties are plotted. Upper panel: Mean branching ratios $\langle b_0 \rangle$ determined from the present results (black data points) and extracted from statistical model calculations (red solid line) with its 1σ uncertainty band (red dotted lines) taken from [21].

horizontally ($i = \text{hor}$) with respect to the polarization plane, the corresponding unfolded spectra were integrated in the region where the beam intensity is above 10% of its maximum. This region has been varied together with parameters within the unfolding procedure (as mentioned before) in order to derive systematic errors for the extracted cross sections. By this integration, resolved peaks as well as so-called unresolved contributions are included.

The average asymmetry ϵ is defined by

$$\epsilon = \frac{A^{\text{hor}}_{0\to x\to 0} - A^{\text{ver}}_{0\to x\to 0}}{A^{\text{hor}}_{0\to x\to 0} + A^{\text{ver}}_{0\to x\to 0}} \tag{4}$$

and is presented in the upper panel of Fig. 5, together with the expected values of the angular distributions for $E1$ and $M1$ ground-state transitions, respectively. The latter are determined via simulations and are also used in Eq. (2). The results for the elastic cross section separated by $E1$ and $M1$ contribution are given in the lower panel of Fig. 5. As mentioned before, the $E1$ cross section is dominant at all excitation energies. The separation into $E1$ and $M1$ contributions is only possible for the elastic part of the cross section. With the method to extract the inelastic cross section one cannot discriminate between the two contributions and there is no reason to assume that the branching of the initially populated $J^\pi = 1^-$ and $J^\pi = 1^+$ states is the same.

The results for the elastic, inelastic and total cross sections are shown in the lower panel of Fig. 6. At low excitation energy, $\sigma_{\gamma\gamma'}$ hardly contributes to the total photoabsorption cross section, while it continuously increases towards 10 MeV. As in other cases, the inelastic cross section exhibits fewer structures when compared to the elastic cross section, which is probably mostly driven by strong single excitations. The present results are compared to those from Ref. [21] which have been obtained by using the data from NRF experiments with bremsstrahlung. It is obvious that, towards 10 MeV, there is an increasing discrepancy between the two data sets. At 10 MeV, the present value for the total photoabsorption cross section is only about half of that reported in [21].

An important quantity needed within the analysis in [21] is the decay pattern of the excited states involved. In [21], this is modeled by simulations of statistical γ-ray cascades using the code γDEX [24,45]. With the present data, the average ground-state branching ratio $\langle b_0 \rangle = \sigma_{\gamma\gamma}/\sigma_\gamma$ can be determined experimentally as a function of the excitation energy. The upper panel of Fig. 6 compares the data to the corresponding values of the cascade simulations used in [21]. While the shapes roughly agree, the absolute simulated values amount on average to about 60% of the experimental ones. This difference explains a large fraction of the discrepancy between the cross sections extracted in the present analysis and in the statistical analysis of the bremsstrahlung data

TABLE I. Total photoabsorption cross section σ_γ, average ground-state branching ratio $\langle b_0 \rangle$ and the ratio of $M1$ to $E1$ elastic cross section deduced within the present analysis. For σ_γ, statistical and systematic uncertainties are given separately.

E_x[MeV]	σ_γ[mb] ($\pm$ stat.) ($\pm$ syst.)	$\langle b_0 \rangle$	$M1/E1$
5.60	0.61(5)(2)	0.74(4)	0.18(4)
5.75	1.64(6)(6)	0.81(3)	0.07(1)
5.90	1.86(9)(7)	0.86(3)	0.03(1)
6.10	0.93(5)(3)	0.74(4)	0.12(2)
6.30	0.53(4)(5)	0.65(6)	0.14(6)
6.50	0.77(6)(6)	0.58(8)	0.11(4)
6.70	1.51(7)(10)	0.70(6)	0.10(2)
6.90	2.27(10)(10)	0.75(4)	0.10(2)
7.10	2.35(11)(6)	0.74(3)	0.09(2)
7.30	3.28(11)(17)	0.77(5)	0.08(2)
7.50	3.49(15)(12)	0.72(3)	0.11(1)
7.70	3.86(13)(17)	0.70(4)	0.11(1)
7.90	3.53(12)(16)	0.64(4)	0.24(4)
8.15	3.78(13)(17)	0.55(4)	0.21(3)
8.40	4.72(17)(16)	0.53(3)	0.23(3)
8.65	5.42(18)(29)	0.59(4)	0.14(3)
8.90	6.92(22)(36)	0.57(4)	0.19(4)
9.15	6.71(22)(15)	0.54(2)	0.20(2)
9.40	5.96(20)(22)	0.49(3)	0.13(2)
9.65	6.40(21)(23)	0.53(3)	0.09(2)
9.90	5.82(19)(16)	0.62(2)	0.11(2)

taken at γELBE. Moreover, this demonstrates the importance of the determination of model-independent branching ratios and, hence, photoabsorption cross sections below the neutron-separation energy. However, the region above 10 MeV was not covered in the experiment at HIγS. The experimental results for σ_γ, $\langle b_0 \rangle$, and the ratio of the $M1$ to $E1$ elastic cross sections are summarized in Table I.

V. CONCLUSIONS

We have determined the photoabsorption cross sections of ^{66}Zn in the energy range between 5.6 and 10 MeV using NRF data taken with a quasi-monoenergetic and linearly polarized photon beam at HIγS. While the monoenergetic character of the beam allows to extract the full elastic as well as inelastic cross sections, the high degree of linear polarization enables for a separation of the $E1$ and $M1$ contributions to the elastic cross sections.

Above about 8 MeV, the determined total photoabsorption cross sections are considerably smaller than the ones obtained from statistical-model calculations applied to the interpretation of NRF experiments using continuous-energy bremsstrahlung, only. The discrepancy is increasing with excitation energy to about a factor of two at 10 MeV. One of the important ingredients in the analysis of the bremsstrahlung data is the decay behavior of the photoexcited states, which in that case is estimated through simulations of statistical γ-ray cascades. Within the present analysis, the average ground-state branching ratios $\langle b_0 \rangle$ are deduced from experimental intensities, and are larger than the simulated ones by about 60%. This partly explains the differences between the present cross sections and the ones from the bremsstrahlung experiment. However, a small amount of the intensity of inelastic transitions bypassing the low-energy excited states states may be missing in the present analysis.

These differences may indicate that certain inputs to the statistical model, such as nuclear level densities, are not well described in nuclei around $A = 60$. For heavier nuclei, there are examples of better agreement between simulated and experimental branching ratios and cross sections [24,46], but discrepancies have also been reported before [28,29]. Altogether, as shown here for ^{66}Zn, combined experiments provide the possibility to determine scattering cross sections of resolved transitions over a wide energy range using bremsstrahlung and to determine model-independent continuous photoabsorption cross sections using LCB photon beams.

VI. DATA AVAILABILITY

The datasets obtained in the experiments and used for analysis in the current study are available from the corresponding author on reasonable request. The generated results presented in this article are openly available and published in the TUdatalib data repository of Technische Universität Darmstadt [47].

ACKNOWLEDGMENTS

The authors thank the HIγS accelerator staff for providing excellent LCB photon beams and experimental conditions. R.M. acknowledges support by the U.S. Department of Energy, Office of Science, Office of Nuclear Physics under Grant No. LANLEM77. The UWS group acknowledges financial support from UK STFC (Grant No. ST/P005101/1). J.S. acknowledges financial support by the UK Nuclear Data Network. T.B. and V.W. acknowledge support by the BMBF Grant No. 05P21RDEN9 and J.W. acknowledges support by the BMBF Grant No. 05P18PKEN9. T.B., U.F.-G., J. K., and O.P. are supported by the Deutsche Forschungsgemeinschaft (DFG, German Research Foundation) – Project-ID 279384907 – SFB1245. J.I., J.K., and O.P. are supported by the grant "Nuclear Photonics" within the LOEWE program of the State of Hesse. J.I. and N.P. acknowledge the support by the State of Hesse within the Research Cluster ELEMENTS (Project ID No. 500/10.006). The remaining authors are supported by the US DOE, office of science, office of nuclear physics under Grants No. DE-FG02-97ER41033 (TUNL) and DE-FG02-97ER41041 (UNC).

[1] W. Hauser and H. Feshbach, Phys. Rev. **87**, 366 (1952).

[2] S. Goriely, P. Dimitriou, M. Wiedeking, T. Belgya, R. Firestone, J. Kopecky, M. Krtička, V. Plujko, R. Schwengner, S. Siem,

H. Utsunomiya, S. Hilaire, S. Péru, Y. S. Cho, D. M. Filipescu, N. Iwamoto, T. Kawano, V. Varlamov, and R. Xu, Eur. Phys. J. A **55**, 172 (2019).
[3] A. Larsen, A. Spyrou, S. Liddick, and M. Guttormsen, Prog. Part. Nucl. Phys. **107**, 69 (2019).
[4] A. Zilges, D. Balabanski, J. Isaak, and N. Pietralla, Prog. Part. Nucl. Phys. **122**, 103903 (2022).
[5] D. Savran, T. Aumann, and A. Zilges, Prog. Part. Nucl. Phys. **70**, 210 (2013).
[6] A. Bracco, E. G. Lanza, and A. Tamii, Prog. Part. Nucl. Phys. **106**, 360 (2019).
[7] F. Bauwens, J. Bryssinck, D. De Frenne, K. Govaert, L. Govor, M. Hagemann, J. Heyse, E. Jacobs, W. Mondelaers, and V. Y. Ponomarev, Phys. Rev. C **62**, 024302 (2000).
[8] M. Scheck, V. Y. Ponomarev, T. Aumann, J. Beller, M. Fritzsche, J. Isaak, J. H. Kelley, E. Kwan, N. Pietralla, R. Raut, C. Romig, G. Rusev, D. Savran, K. Sonnabend, A. P. Tonchev, W. Tornow, H. R. Weller, and M. Zweidinger, Phys. Rev. C **87**, 051304(R) (2013).
[9] M. Scheck, V. Y. Ponomarev, M. Fritzsche, J. Joubert, T. Aumann, J. Beller, J. Isaak, J. H. Kelley, E. Kwan, N. Pietralla, R. Raut, C. Romig, G. Rusev, D. Savran, L. Schorrenberger, K. Sonnabend, A. P. Tonchev, W. Tornow, H. R. Weller, A. Zilges *et al.*, Phys. Rev. C **88**, 044304 (2013).
[10] G. Rusev, R. Schwengner, R. Beyer, M. Erhard, E. Grosse, A. R. Junghans, K. Kosev, C. Nair, K. D. Schilling, A. Wagner, F. Dönau, and S. Frauendorf, Phys. Rev. C **79**, 061302(R) (2009).
[11] R. Schwengner, R. Massarczyk, G. Rusev, N. Tsoneva, D. Bemmerer, R. Beyer, R. Hannaske, A. R. Junghans, J. H. Kelley, E. Kwan, H. Lenske, M. Marta, R. Raut, K. D. Schilling, A. Tonchev, W. Tornow, and A. Wagner, Phys. Rev. C **87**, 024306 (2013).
[12] A. Makinaga, R. Massarczyk, M. Beard, R. Schwengner, H. Otsu, T. Al-Abdullah, M. Anders, D. Bemmerer, R. Hannaske, R. John, A. R. Junghans, S. E. Müller, M. Röder, K. Schmidt, and A. Wagner, Phys. Rev. C **94**, 044304 (2016).
[13] J. Wilhelmy, M. Müscher, G. Rusev, R. Schwengner, R. Beyer, M. Bhike, P. Erbacher, F. Fiedler, U. Friman-Gayer, J. Glorius, R. Greifenhagen, S. Hammer, T. Hensel, J. Isaak, A. R. Junghans, Krishichayan, B. Löher, S. E. Müller, N. Pietralla, S. Reinicke, D. Savran, P. Scholz, K. Sonnabend, T. Szucs, M. Tamkas, W. Tornow, S. Turkat, A. Wagner, and A. Zilges, Phys. Rev. C **102**, 044327 (2020).
[14] H. Pai, J. Beller, N. Benouaret, J. Enders, T. Hartmann, O. Karg, P. von Neumann-Cosel, N. Pietralla, V. Y. Ponomarev, C. Romig, M. Scheck, L. Schnorrenberger, S. Volz, and M. Zweidinger, Phys. Rev. C **88**, 054316 (2013).
[15] Krishichayan, M. Bhike, W. Tornow, G. Rusev, A. P. Tonchev, N. Tsoneva, and H. Lenske, Phys. Rev. C **91**, 044328 (2015).
[16] T. Shizuma, T. Hayakawa, I. Daito, H. Ohgaki, S. Miyamoto, and F. Minato, Phys. Rev. C **96**, 044316 (2017).
[17] J. Wilhelmy, B. A. Brown, P. Erbacher, U. Gayer, J. Isaak, Krishichayan, B. Löher, M. Müscher, H. Pai, N. Pietralla, P. Ries, D. Savran, P. Scholz, M. Spieker, W. Tornow, V. Werner, and A. Zilges, Phys. Rev. C **98**, 034315 (2018).
[18] P. C. Ries, H. Pai, T. Beck, J. Beller, M. Bhike, V. Derya, U. Gayer, J. Isaak, B. Löher, Krishichayan, L. Mertes, N. Pietralla, C. Romig, D. Savran, M. Schilling, W. Tornow, S. Typel, V. Werner, J. Wilhelmy, A. Zilges, and M. Zweidinger, Phys. Rev. C **100**, 021301(R) (2019).
[19] R. Schwengner, R. Beyer, F. Dönau, E. Grosse, A. Hartmann, A. Junghans, S. Mallion, G. Rusev, K. Schilling, W. Schulze, and A. Wagner, Nucl. Instrum. Methods Phys. Res. A **555**, 211 (2005).
[20] H. R. Weller, M. W. Ahmed, H. Gao, W. Tornow, Y. K. Wu, M. Gai, and R. Miskimen, Prog. Part. Nucl. Phys. **62**, 257 (2009).
[21] R. Schwengner, R. Massarczyk, M. Scheck, W. Tornow, G. Battaglia, T. Beck, D. Bemmerer, N. Benouaret, R. Beyer, M. Butterling, F. Fiedler, S. W. Finch, C. Fransen, U. Friman-Gayer, A. Frotscher, R. Gonzalez, M. Grieger, A. Hartmann, T. Hensel, E. Hoemann, H. Hoffmann, R. V. F. Janssens, S. Johnson, M. D. Jones, A. R. Junghans, N. Kelly, J. Kleemann, Krishichayan D. R. Little, F. Ludwig, S. E. Muller, D. ODonnell, O. Papst, E. Pirovano, J. Sinclair, M. P. Takacs, S. Turkat, S. Urlass, A. Wagner, V. Werner, O. Wieland, and J. Wilhelmy, Phys. Rev. C **103**, 024312 (2021).
[22] R. Schwengner, G. Rusev, N. Benouaret, R. Beyer, M. Erhard, E. Grosse, A. R. Junghans, J. Klug, K. Kosev, L. Kostov, C. Nair, N. Nankov, K. D. Schilling, and A. Wagner, Phys. Rev. C **76**, 034321 (2007).
[23] G. Rusev, R. Schwengner, F. Dönau, M. Erhard, E. Grosse, A. R. Junghans, K. Kosev, K. D. Schilling, A. Wagner, F. Bečvář, and M. Krtička, Phys. Rev. C **77**, 064321 (2008).
[24] R. Massarczyk, R. Schwengner, F. Dönau, E. Litvinova, G. Rusev, R. Beyer, R. Hannaske, A. R. Junghans, M. Kempe, J. H. Kelley, T. Kögler, K. Kosev, E. Kwan, M. Marta, A. Matic, C. Nair, R. Raut, K. D. Schilling, G. Schramm, D. Stach *et al.*, Phys. Rev. C **86**, 014319 (2012).
[25] R. Schwengner, R. Massarczyk, R. Beyer, M. Bhike, B. A. Brown, Krishichayan, K. Sieja, W. Tornow, D. Bemmerer, M. Butterling, V. Derya, M. Dietz, F. Fiedler, U. Friman-Gayer, A. Frotscher, M. Grieger, A. Hartmann, A. R. Junghans, T. Kögler, F. Ludwig, B. Lutz, H. Pai, T. Szucs, M. P. Takacs, and A. Wagner, Phys. Rev. C **101**, 064303 (2020).
[26] M. Müscher, J. Wilhelmy, R. Massarczyk, R. Schwengner, M. Grieger, J. Isaak, A. R. Junghans, T. Kögler, F. Ludwig, D. Savran, D. Symochko, M. P. Takács, M. Tamkas, A. Wagner, and A. Zilges, Phys. Rev. C **102**, 014317 (2020).
[27] A. P. Tonchev, S. L. Hammond, J. H. Kelley, E. Kwan, H. Lenske, G. Rusev, W. Tornow, and N. Tsoneva, Phys. Rev. Lett. **104**, 072501 (2010).
[28] J. Isaak, D. Savran, M. Krticka, M. W. Ahmed, J. Beller, E. Fiori, J. Glorius, J. H. Kelley, B. Löher, N. Pietralla, C. Romig, G. Rusev, M. Scheck, L. Schnorrenberger, J. Silva, K. Sonnabend, A. P. Tonchev, W. Tornow, H. R. Weller, and M. Zweidinger, Phys. Lett. B **727**, 361 (2013).
[29] C. Romig, J. Beller, J. Glorius, J. Isaak, J. H. Kelley, E. Kwan, N. Pietralla, V. Y. Ponomarev, A. Sauerwein, D. Savran, M. Scheck, L. Schnorrenberger, K. Sonnabend, A. P. Tonchev, W. Tornow, H. R. Weller, A. Zilges, and M. Zweidinger, Phys. Rev. C **88**, 044331 (2013).
[30] P. M. Goddard, N. Cooper, V. Werner, G. Rusev, P. D. Stevenson, A. Rios, C. Bernards, A. Chakraborty, B. P. Crider, J. Glorius, R. S. Ilieva, J. H. Kelley, E. Kwan, E. E. Peters, N. Pietralla, R. Raut, C. Romig, D. Savran, L. Schnorrenberger, M. K. Smith *et al.*, Phys. Rev. C **88**, 064308 (2013).
[31] J. Isaak, D. Savran, B. Löher, T. Beck, M. Bhike, U. Gayer, Krishichayan, N. Pietralla, M. Scheck, W. Tornow, V. Werner, A. Zilges, and M. Zweidinger, Phys. Lett. B **788**, 225 (2019).
[32] J. Isaak, D. Savran, B. Löher, T. Beck, U. Friman-Gayer, Krishichayan, N. Pietralla, V. Y. Ponomarev, M. Scheck,

W. Tornow, V. Werner, A. Zilges, and M. Zweidinger, Phys. Rev. C **103**, 044317 (2021).

[33] B. Löher, V. Derya, T. Aumann, J. Beller, N. Cooper, M. Duchene, J. Endres, E. Fiori, J. Isaak, J. Kelley, M. Knörzer, N. Pietralla, C. Romig, D. Savran, M. Scheck, H. Scheit, J. Silva, A. P. Tonchev, W. Tornow, H. Weller *et al.*, Nucl. Instrum. Methods Phys. Res. A **723**, 136 (2013).

[34] N. Pietralla, Z. Berant, V. N. Litvinenko, S. Hartman, F. F. Mikhailov, I. V. Pinayev, G. Swift, M. W. Ahmed, J. H. Kelley, S. O. Nelson, R. Prior, K. Sabourov, A. P. Tonchev, and H. R. Weller, Phys. Rev. Lett. **88**, 012502 (2001).

[35] M. Tamkas, E. Açıksöz, J. Isaak, T. Beck, N. Benouaret, M. Bhike, I. Boztosun, A. Durusoy, U. Gayer, Krishichayan, B. Löher, N. Pietralla, D. Savran, W. Tornow, V. Werner, A. Zilges, and M. Zweidinger, Nucl. Phys. A **987**, 79 (2019).

[36] O. Papst, V. Werner, J. Isaak, N. Pietralla, T. Beck, C. Bernards, M. Bhike, N. Cooper, B. P. Crider, U. Friman-Gayer, J. Kleemann, Krishichayan, B. Löher, F. Naqvi, E. E. Peters, F. M. Prados-Estévez, R. S. Ilieva, T. J. Ross, D. Savran, W. Tornow, and J. R. Vanhoy, Phys. Rev. C **102**, 034323 (2020).

[37] U. Friman-Gayer, J. Kleemann, and O. Papst, GEANT4 simulation of the Upstream Target Room (UTR) at the HIγS facility (2019), available at https://github.com/uga-uga/utr.

[38] S. Agostinelli, J. Allison, K. Amako, J. Apostolakis, H. Araujo, P. Arce, M. Asai, D. Axen, S. Banerjee, G. Barrand, F. Behner, L. Bellagamba, J. Boudreau *et al.*, Nucl. Instrum. Methods Phys. Res. A **506**, 250 (2003).

[39] J. Allison, K. Amako, J. Apostolakis, H. Araujo, P. Arce Dubois, M. Asai, G. Barrand, R. Capra, S. Chauvie, R. Chytracek, G. A. P. Cirrone, G. Cooperman, G. Cosmo, G. Cuttone, G. G. Daquino, M. Donszelmann, M. Dressel, G. Folger, F. Foppiano, J. Generowicz *et al.*, IEEE Trans. Nucl. Sci. **53**, 270 (2006).

[40] J. Allison, K. Amako, J. Apostolakis, P. Arce, M. Asai, T. Aso, E. Bagli, A. Bagulya, S. Banerjee, G. Barrand, B. Beck, A. Bogdanov, D. Brandt, J. Brown, H. Burkhardt, P. Canal, D. Cano-Ott, S. Chauvie, K. Cho, G. Cirrone *et al.*, Nucl. Instrum. Methods Phys. Res. A **835**, 186 (2016).

[41] D. Savran, M. Fritzsche, J. Hasper, K. Lindenberg, S. Müller, V. Y. Ponomarev, K. Sonnabend, and A. Zilges, Phys. Rev. Lett. **100**, 232501 (2008).

[42] B. Löher, D. Savran, T. Aumann, J. Beller, M. Bhike, N. Cooper, V. Derya, M. Duchene, J. Endres, A. Hennig, P. Humby, J. Isaak, J. Kelley, M. Knörzer, N. Pietralla, V. Ponomarev, C. Romig, M. Scheck, H. Scheit, J. Silva *et al.*, Phys. Lett. B **756**, 72 (2016).

[43] J. Isaak, Investigation of decay properties of the pygmy Dipole Resonance and photon strength functions on excited states in $(\gamma, \gamma'\gamma'')$ reactions, PhD thesis, Johannes Gutenberg-Universität Mainz (2016).

[44] U. Friman-Gayer, J. Kleemann, and O. Papst, Horst - Histogram original reconstruction spectrum tool (2022), available at https://github.com/uga-uga/Horst.

[45] G. Schramm, R. Massarczyk, A. R. Junghans, T. Belgya, R. Beyer, E. Birgersson, E. Grosse, M. Kempe, Z. Kis, K. Kosev, M. Krtička, A. Matic, K. D. Schilling, R. Schwengner, L. Szentmiklósi, A. Wagner, and J. L. Weil, Phys. Rev. C **85**, 014311 (2012).

[46] R. Massarczyk, G. Rusev, R. Schwengner, F. Dönau, C. Bhatia, M. E. Gooden, J. H. Kelley, A. P. Tonchev, and W. Tornow, Phys. Rev. C **90**, 054310 (2014).

[47] D. Savran, J. Isaak, R. Schwengner, R. Massarczyk, M. Scheck, W. Tornow, G. Battaglia, T. Beck, S. W. Finch, C. Fransen, U. Friman-Gayer, R. Gonzalez, E. Hoemann, R. V. F. Janssens, S. R. Johnson, M. D. Jones, J. Kleemann, Krishichayan, D. R. Little, D. O'Donnell *et al.*, TUdatalib, Technische Universität Darmstadt (2022), https://doi.org/10.48328/tudatalib-935.